

Jasmina Dedić¹
Dragan Lazarević
Bogdan Nedić
Milan Mišić
Živče Šarkočević

DEVELOPMENT OF THE MATHEMATICAL MODEL FOR SURFACE TOPOGRAPHY QUALITY DETERMINATION AT THE END MILLING PROCESS

Article info:
Received 25.12.2016
Accepted 07.04.2017

UDC – 005.6:621.7
DOI – 10.18421/IJQR11.02-01

Abstract: As a metal machining process, end milling is the most widely used processes in industry. One of the most important indicators of success in finishing operation is the estetic quality of the surface that is directly connected to the maximal height of uneven surfaces, namely roughness. In process of milling the quality of the machined surface depends of many factors, for example, tool geometry, cutter parallel axis offset and cutter axis tilt, tool deflection due to cutting forces, tool and work piece vibrations etc. This paper presents the development of mathematical model for the determination of the quality of the machined surface topography. The model starts from an ideal trochoid point trajectory on the cutting edge tooth end mill, and then inserts the deviations due to cutter parallel axis offset and cutter axis tilt and gives instructions for the input of other factors that influence on the machined surface quality. Also it compares the values of maximal roughness height with different mill axis positions, and on different mill cross section heights, as well as the differences at up and down milling.

Keywords: end milling, surface quality, cutting edge trajectory

1. Introduction

As a metal machining process, end milling is the most widely used processes in industry. Peripheral milling is a common removal operation of metals that are used in car, aeroplane and production industries. One of the most important indicators of success in finish operations is the aesthetic quality of the surface. As the quality requirements raise, the emphasis is placed on surface's aesthetic quality. One of the factors that can

degrade the surface aesthetic quality is the so-called "tool setting error" that occurs when the tool axis doesn't match the rotating spindle axis. Tooling errors can be observed as the sum of two kinds of errors: errors due to cutter parallel axis offset and errors due to the cutter axis tilt between tool axis and spindle axis. The second factor is the error due to the deviation of measures of the mill tooth radius.

Pioneer work on analytical determining of the cutting edge tool path in milling operations was given by Martellotti (1941). He brought up the parametric equations with trochoidal toolpath cutting tool edges and evaluated the elements such as the curvature

¹ Corresponding author: Jasmina Dedić
email: jasminavdedic@hotmail.com

radius of the tooth path, clearance and rake angles, tooth path lengths, radial thickness of the chip and their effect on the milled surface quality, power consumed, and the cutter life. Kline et al. (Kline et al., 1982; Kline and DeVor, 1983) study the error influence due to the cutter parallel axis offset on the tool teeth marks that due to the machining stay on the work piece surface. They allege the generation of the heterogeneity band and the concept of effective radius and develop the model for cutting geometry calculation and prediction of cutting forces with the cutter parallel axis offset effect of the work piece made out of aluminum 7075. Babin et al. (Babin et al., 1985; Babin et al., 1986) developed the cutting model with cutter parallel axis which they added tool deflection due to cutting forces as well as the influence of cutter parallel axis offset on the surface roughness value change for different milling surface heights at different spindle speeds to. Ismail et al. (1993), performed the model taking into consideration cutter parallel axis offsets and included the effects of mill vibration and flank face wear and analyzed the irregularities in feed marks. Schmitz et al. (2007), investigates the effect of cutter parallel axis offset on milling surface topography, surface location error, and stability in end milling. Li and Li (2005) found that the change of cutter radius for a tooth relative to its preceding one is the most important factor in evaluating the effects of cutter runout. Gao et al. (2006) developed mesh-independent direct computing method. The simulation of machined surface topography is carried out for both end and ball-end milling processes. Stori et al. (1999) besides cutter parallel axis offsets take into consideration cutter axis tilt and perform machining parameter optimization for peripheral finish milling operations. Raganath and Sutherland (2002) present a three-step methodology for runout estimation, including cutter grind, parallel axis offset, and cutter tilt in peripheral milling. Ryu et al. (2003) cutting forces and

tool deflections are calculated considering tool geometry, tool setting error (parallel axis offset and cutter tilt) and machine tool stiffness in side wall machining under various cutting conditions generally used in die and mold manufacturing. Also the characteristics and the difference of generated surface shape in up milling and down milling are discussed.

Omar et al. (2007) developed the model that includes the effects of tool runout (parallel axis offset and cutter tilt), tool deflection, system dynamics, flank face wear, and the tool tilting on the surface roughness. Ehmann and Hong (1994) develop the model (called surface-shaping system) for prediction of the topography of the milled surface over the influence of tool runout, machine deformation and vibration, as well as higher order motions over transformation matrixes. Arizmendi et al. (2009a) placed the general model for tool path end mill determination over transformation matrixes, taking in consideration parallel axis offset and cutter tilt. They comprehensively analyze the occurrence of roughness heterogeneity bands on milled surfaces. In the next work Arizmendi et al. (2009b) in the model equations of the cutting edge paths added tool vibrates during the cutting process. The model allows prediction of the topography, the roughness values and the form errors of the milled surfaces. Arizmendi et al. (2010a; 2010b) performed model effects of two factors that produce tool runout: tool setting errors and cutter grinding errors. They continue to analyze heterogeneity bands in the new-occurring conditions as well.

2. Martellotti's model for generating surface topography obtained with peripheral

Milling is the process of removing material from a workpiece in shape of small individual chips. These chips are forming with occasional involvement of a multitude

of blades or teeth as the integral tool piece, or inlaid tiles in cylindrical body known as mill, with a workpiece. This periodical involvement is the product of extra movement of the work piece in the area that is dominated by cutting tool rotation.

As said, the first work on an analytical determination of the tool path in milling operation was given by Martellotti. He brought the parametric equations with trochoidal tool path cutting edges. For the needs of analysis, the system that consists with a rotating mill and a workpiece that is translationally moving, replaced with an equivalent system in whom the work piece is static, and the cutting tool is simultaneously rotating and moving translationally. In this case, the direction of the translational movement of the cutting tool will be opposite of the work piece movement, that is obtained in a common scenario. Idealized version of this model (Figure 1), is consisted with a pinion of correct dimensions connected with an operating stem on which is the mill set. The pinion is coupled with a rack solidly connected to the static machine basis. After the spindle rotation, the cutting tool will move to the work piece for the feed value.

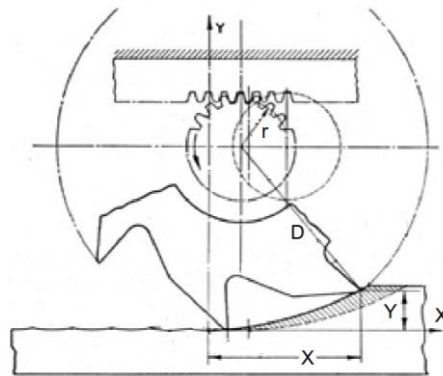


Figure 1. Rack-and-pinion model (Martellotti, 1941)

The movement direction of the point tool is constantly changing relatively to the movement direction of the work piece, so the path of the tooth, that derives from this, is not circular, but a curve that is correctly outlined as a curtate trochoid. The extended cycloid is outlined by the solid point A that is laying outside the circle (Figure 2), that without gliding is rolling on a solid direction X. In the case that the point B is placed on the extent of the circle, the resulting curve is cycloid. The third type of a curve is a prolate trochoid, and it occurs if the point C is laying inside the circle.

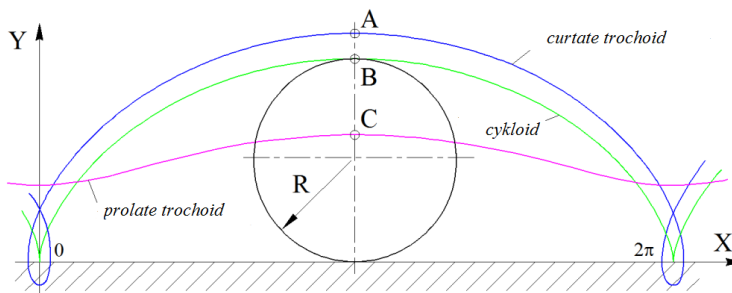


Figure 2. Family of the cycloid curves

Because of the limitations of the period of involvement of every tooth, the milled scraping is short and varying thickness, while the processed surface consists of series of elementary surfaces occurring by individual blade cutting tool, while the surface

topography is formed with mill traces, produced on a milled surface by different cutting edges of a cutter spindle with its trochoidal paths. Consider the ideal case where all the points of all of the tool cutting edges are placed on a cylindrical surface

coaxial with the spindle axis. In that case, the tooth marks would contain trochoidal arcs of the same length, separated along the

feed directions with distance equal to one feed per tooth fz and the difference in depth h (Figure 3).

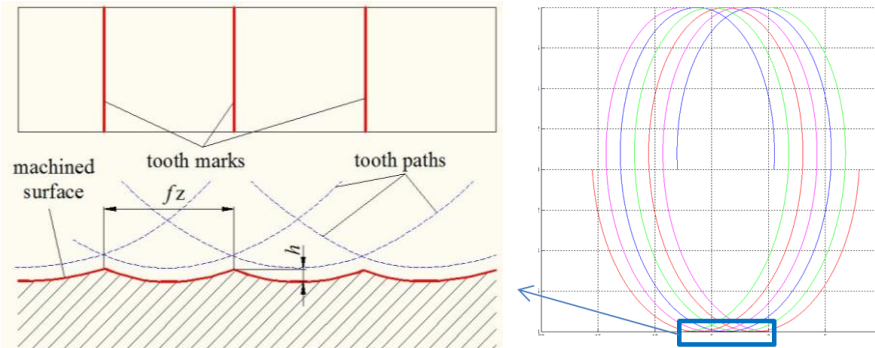


Figure 3. Ideal case of the topography of the milled surface

Up milling (UM) and down milling (DM) don't use the same part of trochoidal tooth path while cutting because of different rotational moving tool directions, as presented on figure 4. At DM, the tooth mark height (height of roughness) marked with h_{down} is larger then the one at UM, h_{up} obtained with the same feed. Thus is the roughness bigger at DM then at UM (Martelloti, 1941). The roughness height (h) is connected to the feed per tooth (fz), cutting tool radius (R), and the number of tooth (z)

and can be determined from the next expression (Dotcheva et al., 2013):

$$h = \frac{f_z^2}{8 \left(R \pm \frac{f_z \cdot z}{\pi} \right)}$$

The positive sign in the detorminator is for up milling, and then negative sign is for down milling. This equation implies the toothstep equality by the extent of the cutting tool and machining without run-out.

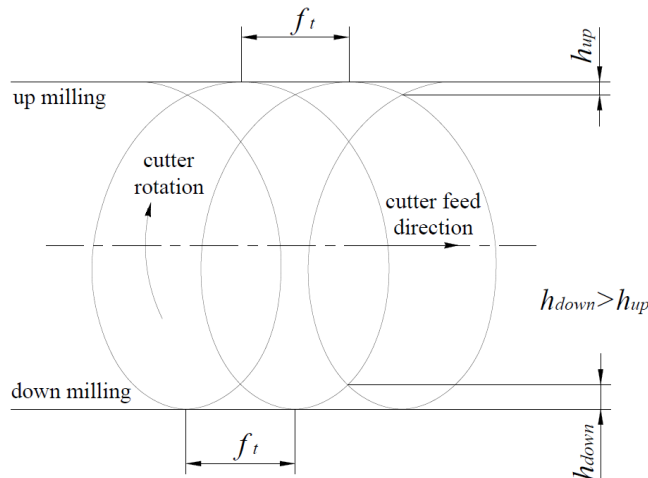


Figure 4. Trochoidal tool path in up and down-milling (Dotcheva et al., 2013)

Experience shows that, when the cutter spindle tightens into tool carrier, all the points on cutting edges aren't really placed in the same cylinder because of the fact that mill axis isn't matched with the spindle axis, and that the heights of all teeth aren't the same. As a result, every point of the cutting edge is rotating around the spindle with so-called effective radius differentiated from the nominal. How every cutting edge has a different effective radius, the tooth marks will be contained out of trochoid arcs of different lengths that will repeat with the period equal with one feed per turn f where $f = N_t \cdot fz$, and N_t milling tooth count. Therefore, to predict topography of the milled surface and the influence of radial deviations of the cutting edge radius, the position of

cutting edge points relative to the spindle axis must be known, and then first to take into account the geometry of the tooling error.

3. Model that takes in consideration the errors of setting a mill in a tool holder

Figure 5 shows the geometry of a spindle end mill and its connected system $X_T Y_T Z_T$. The spindle end mill is modeling with N_t spiral cutting edges that are located on the periphery of a cylindrical surface with nominal radius R shown on the figure 5.

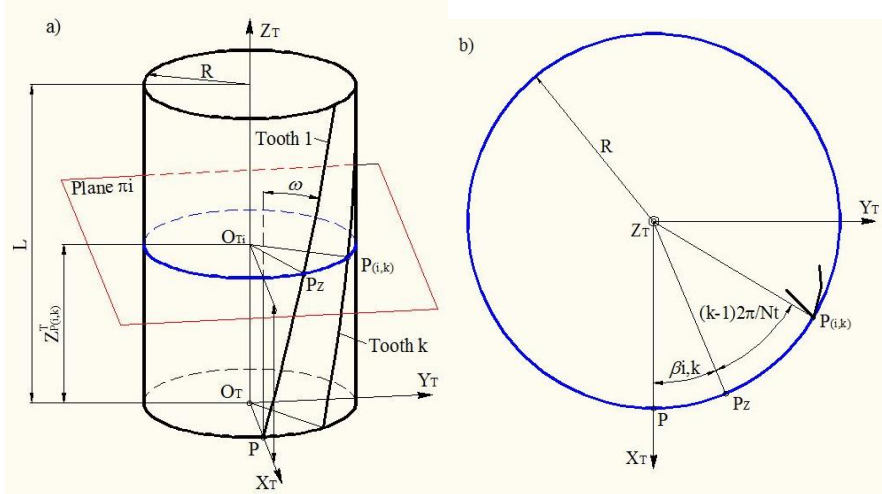


Figure 5. Geometry of the end mill (Arizmendi et al., 2009b)

To the calculation of ideal point path on a cutting edge can be found by placing the plane normal to the axis Z_T of the mill on height $z_{P(i,k)}^T$ from the top point O_T (Figure 5-a). This plane cuts the tooth 1 and k in points P_z and $P_{(i,k)}$, respectively. Viewed from the top on the plane (Figure 5-b), angle position $\beta_{i,k}$ in comparison to the lowest tooth point 1, P , can be written the next:

$$\beta_{(i,k)} = \frac{z_{P(i,k)}^T \cdot \tan(\omega)}{R} \quad (1)$$

where ω is the helical angle.

Now the coordinates $(x_{P(i,k)}^T, y_{P(i,k)}^T, z_{P(i,k)}^T)$ and points $P_{(i,k)}$ can be presented with calculations:

$$\begin{aligned} x_{P(i,k)}^T &= R \cdot \cos \left[\beta_{(i,k)} + (k-1) \frac{2\pi}{N_t} \right] \\ y_{P(i,k)}^T &= R \cdot \sin \left[\beta_{(i,k)} + (k-1) \frac{2\pi}{N_t} \right] \\ z_{P(i,k)}^T &= \frac{\beta_{(i,k)} R}{\tan(\omega)} \end{aligned} \quad (2)$$

Where k is the ordinal tooth number, and that $k=1,2,\dots,N_t$, a N_t , and N_t tooth number count. In order to obtain calculations that describe the path of point $P(i,k)$ in comparison to the workpiece, it is needed to take in consideration two referent systems: referent system XYZ (Figure 6-a) fixed to the workpiece and system $X_sY_sZ_s$, that rotates around the spindle axis Z_s with constant angular speed and moving for distance f per revolution in the feed direction (X). It is

assumed that the process is stiff so the errors caused due to tool and workpiece vibration can be neglected. Coordinates (x,y) points $P(i,k)$ in the XYZ system can be written in matrix shape in the angle rotation α function (Figure 6-b). Where $x_{P(i,k)}^{(\alpha)}$ and $y_{P(i,k)}^{(\alpha)}$ are coordinates $P(i,k)$ at the angle of rotation in the direction of feed α and the direction normal to the milled surface, respectively and $z_{P(i,k)}^{(\alpha)}$ is the height along the milled surface.

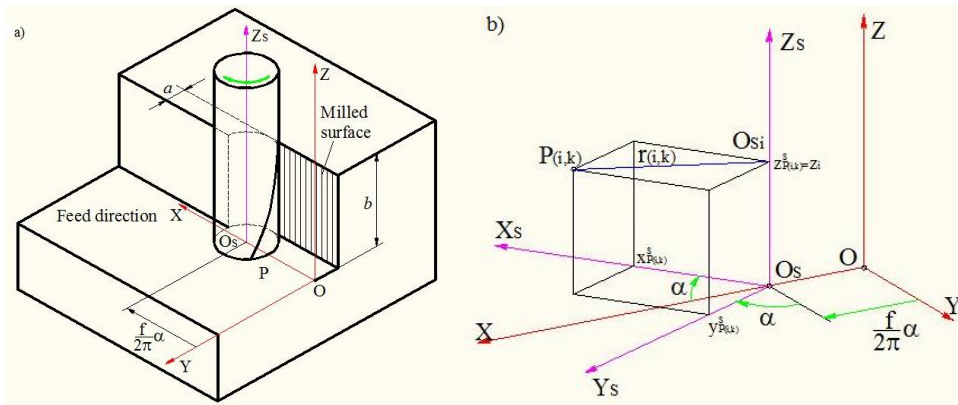


Figure 6. Model's referent systems

Equations of motion point cutting edges with ideal geometry are obtained by entering the

expression for coordinates from equation (2) in the function of equation (3):

$$\begin{bmatrix} x_{P(i,k)}^{(\alpha)} \\ y_{P(i,k)}^{(\alpha)} \\ z_{P(i,k)}^{(\alpha)} \\ 1 \end{bmatrix} = \begin{bmatrix} \cos(\alpha) & \sin(\alpha) & 0 & \frac{f}{2\pi}\alpha \\ -\sin(\alpha) & \cos(\alpha) & 0 & 0 \\ 0 & 0 & 1 & 0 \\ 0 & 0 & 0 & 1 \end{bmatrix} \begin{bmatrix} x_{P(i,k)}^T \\ y_{P(i,k)}^T \\ z_{P(i,k)}^T \\ 1 \end{bmatrix} \quad (3)$$

$$\begin{bmatrix} x_{P(i,k)}^{(\alpha)} \\ y_{P(i,k)}^{(\alpha)} \\ z_{P(i,k)}^{(\alpha)} \\ 1 \end{bmatrix} = \begin{bmatrix} \cos(\alpha) & \sin(\alpha) & 0 & \frac{f}{2\pi}\alpha \\ -\sin(\alpha) & \cos(\alpha) & 0 & 0 \\ 0 & 0 & 1 & 0 \\ 0 & 0 & 0 & 1 \end{bmatrix} \begin{bmatrix} R \cdot \cos \left[\beta_{(i,k)} + (k-1) \frac{2\pi}{N_t} \right] \\ R \cdot \sin \left[\beta_{(i,k)} + (k-1) \frac{2\pi}{N_t} \right] \\ \frac{\beta_{(i,k)} R}{\tan(\omega)} \\ 1 \end{bmatrix} \quad (4)$$

From the figure 4, the relation between angular position $\beta_{i,k}$ and the height of sectional plane $z_i = z_{P(i,k)}^T$ can be brought out:

$$\beta_{(i,k)} = \frac{z_i}{R} \tan(\varpi) \tag{5}$$

$\beta_{(i,k)} \cdot R = z_i \cdot \tan(\varpi)$, where:

Now the definitive equations of point motion in function of rotation angle α are:

$$\begin{bmatrix} x_{P(i,k)}^{(\alpha)} \\ y_{P(i,k)}^{(\alpha)} \\ z_{P(i,k)}^{(\alpha)} \\ 1 \end{bmatrix} = \begin{bmatrix} \cos(\alpha) & \sin(\alpha) & 0 & \frac{f}{2\pi} \alpha \\ -\sin(\alpha) & \cos(\alpha) & 0 & 0 \\ 0 & 0 & 1 & 0 \\ 0 & 0 & 0 & 1 \end{bmatrix} \begin{bmatrix} R \cdot \cos \left[\frac{z_i}{R} \tan(\varpi) + (k-1) \frac{2\pi}{N_t} \right] \\ R \cdot \sin \left[\frac{z_i}{R} \tan(\varpi) + (k-1) \frac{2\pi}{N_t} \right] \\ z_i \\ 1 \end{bmatrix} \tag{6}$$

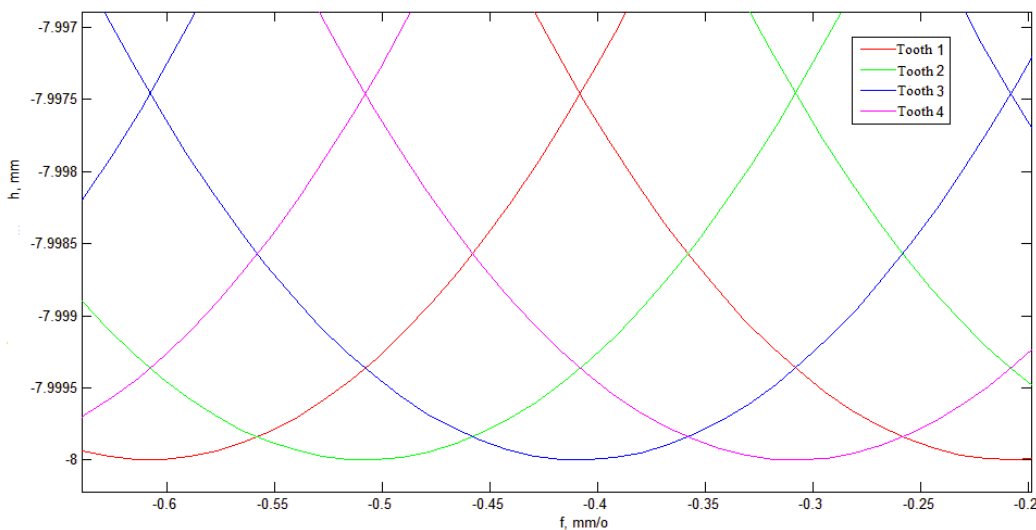


Figure 7. The ideal tooth paths of mills with 4 teeth

On Figure 7, the ideal tooth paths of mills with 4 teeth, radius 8 mm obtained from model and equation (6) are shown.

4. The model that takes into consideration the errors of setting the mill on a topography of a surface

In the order to define a position of a tool axis relative to the axis of spindle, the error of setting the tool (parallel position change of the axis and the axis tilt) is taken into consideration through a series of parameters, points, coordinate systems and planes (Figure 8). The error of setting tools is

defined with parameters used in (Kline and DeVor, 1983; Ranganath and Sutherland, 2202; Arizmendi et al., 2009a). Parallel position change of axis ρ is defined as the distance of central axis of the mill from the spindle axis on a fixed mill end. The tilt of τ is defined as the angle that constructs the mill axis relative to the spindle axis.

In the order to connect both errors (ρ i τ) one with other and with mill edges, it is needed to consider two angles of position (ϕ i λ) (Figure 8-a) over the plane P_T , that contains the tool axis and is parallel with the spindle axis. Besides that, the lowest points of the tooth and mill axis 1, O_T i P , are used respectively. Therefore, angle ϕ is the angle

obtained with plane P_T and the direction ρ given with points A and B on figure 8-a. Angle λ is defined as the angle obtained with a line that connects points P and O_T with the plane P_T counter-clockwise.

Further, through these 4 parameters $\rho, \tau, \phi, \lambda$, the position of every cutting edge point can be defined relatively to the spindle axis. To achieve that, two main coordinate systems have to be established: mill system $X_T Y_T Z_T$, and referent spindle system $X_S Y_S Z_S$ (Figure 8-a):

- System $X_T Y_T Z_T$ is a coordinate system connected to the mill where (1) the axis Z_T matches the mill axis, (2) coordinate start O_T fits the point of intersection of axis Z_T and the free end of the mill and is located at the distance L from the fixed plane, L represents the extension from the toolholder and (3) the axis X_T has the direction of a line that connects the points O_T and P , that is the intersected point of tooth 1 with a free tool end (Figure 8-a).
- System $X_S Y_S Z_S$ is the coordinate system connected to the rotation spindle. In this coordinate system: (1) axis Z_S coincides with the spindle axis, (2) coordinate origin is located on distance L from the fixed plane and (3) axis X_S has the direction of the parallel movement of the mill ρ given by points A and B on figure 8-a.

As well as in literature (Kline and DeVor, 1983; Babin et al., 1985; Stori et al., 1999; Ranganath and Sutherland, 2002; Arizmendi et al., 2009a), in this paper the tool is discretized through plane π_i (Figure 8-a) perpendicular to the rotation axis of spindle Z_S , that is located on height z_i in the system $X_S Y_S Z_S$ and divides it to mutually same distance. Every plane π_i intersects Z_S and Z_T in points O_{S_i} and O_{T_i} respectively and tooth k on cutting edge points $P(i,k)$, where the tooth point k is located on height z_i or $z_{P(i,k)}^S$ in

$X_S Y_S Z_S$ spindle system or on height $z_{P(i,k)}^T$ in system of end mills $X_T Y_T Z_T$. To express coordinate points, the index refers to the observed point, and the exponent to a referent system that it refers to.

To obtain the correlation of points of the cutting edge $P(i,k)$ in the system of spindles $X_S Y_S Z_S$ with its coordinates in the system of mills $X_T Y_T Z_T$, it is needed to take in consideration the additional coordinate systems.

Assisting coordinate systems (Figure 8-b) that are used here are defined by models presented in (Ehmann and Hong, 1994; Arizmendi et al., 2009a):

- System $X_1 Y_1 Z_1$: whose axis are parallel to axis of the spindle system $X_S Y_S Z_S$ but shifted for distance ρ in direction X_S .
- System $X_2 Y_2 Z_2$: obtained by rotating around axis Z_1 of coordinate system $X_1 Y_1 Z_1$ under angle ϕ in counter clockwise direction.
- System $X_3 Y_3 Z_3$: obtained by rotation for angle τ around axis parallel to axis Y_2 and passes through point A in a fixed plane (Figures 8-a,b).

Finally, coordinates $P(i,k)$ in system $X_S Y_S Z_S$ can be expressed as the product of the transformation matrix of coordinates between referent systems previously defined and coordinates of point $P(i,k)$ in system $X_T Y_T Z_T$:

$$\begin{bmatrix} x_{P(i,k)}^S \\ y_{P(i,k)}^S \\ z_{P(i,k)}^S \\ 1 \end{bmatrix} = T_{S1(\rho)} \cdot T_{12(\phi)} \cdot T_{23(L,\tau)} \cdot T_{3T(\lambda)} \begin{bmatrix} x_{P(i,k)}^T \\ y_{P(i,k)}^T \\ z_{P(i,k)}^T \\ 1 \end{bmatrix} \quad (7)$$

Where:

$$T_{S1(\rho)} = \begin{bmatrix} 1 & 0 & 0 & \rho \\ 0 & 1 & 0 & 0 \\ 0 & 0 & 1 & 0 \\ 0 & 0 & 0 & 1 \end{bmatrix}$$

$$T_{12(\phi)} = \begin{bmatrix} \cos(\phi) & -\sin(\phi) & 0 & 0 \\ \sin(\phi) & \cos(\phi) & 0 & 0 \\ 0 & 0 & 1 & 0 \\ 0 & 0 & 0 & 1 \end{bmatrix}$$

$$T_{23(L,\tau)} = \begin{bmatrix} \cos(\tau) & 0 & -\sin(\tau) & L \cdot \sin(\tau) \\ 0 & 1 & 0 & 0 \\ \sin(\tau) & 0 & \cos(\tau) & L \cdot [1 - \cos(\tau)] \\ 0 & 0 & 0 & 1 \end{bmatrix}$$

$$T_{3T(\lambda)} = \begin{bmatrix} \cos(\lambda) & -\sin(\lambda) & 0 & 0 \\ \sin(\lambda) & \cos(\lambda) & 0 & 0 \\ 0 & 0 & 1 & 0 \\ 0 & 0 & 0 & 1 \end{bmatrix}$$

Where the first index of transformational matrixes (T_{S1} , T_{12} , T_{23} i T_{3T}) refers to the last coordinate system, and the second on the initial system and where $x_{P(i,k)}^T$, $y_{P(i,k)}^T$ i $z_{P(i,k)}^T$ coordinates of points $P(i,k)$ in system $X_T Y_T Z_T$, that are obtained previously by taking in consideration the mill geometry.

From equation (2), to calculate the location of point $x_{P(i,k)}^T$, $y_{P(i,k)}^T$ i $z_{P(i,k)}^T$, taking in consideration errors of setting the mill, the angular position $\beta_{i,k}$ must be known. Replacing equation (2) in equation (7), solves for $z_{P(i,k)}^S$ and taking in consideration that $z_{P(i,k)}^S = z_i$, the next equation in relation with angle $\beta_{i,k}$ i z_i is obtained.

$$R \cdot \cos\left(\lambda + \beta_{(i,k)} + (k-1)\frac{2\pi}{N_i}\right) \sin(\tau) + \frac{R \cdot \cos(\tau)}{\tan(\omega)} \beta_{(i,k)} + L(1 - \cos(\tau)) = z_i \quad (8)$$

Solving equation (8) is complicated but $z_{P(i,k)}^T$ can be approximated with a negligible error with $z_{O_{Ti}}^T$, where from figure 8-c, can be seen that

$$L - z_i = (L - z_{O_n}^T) \cos(\tau) \quad (9)$$

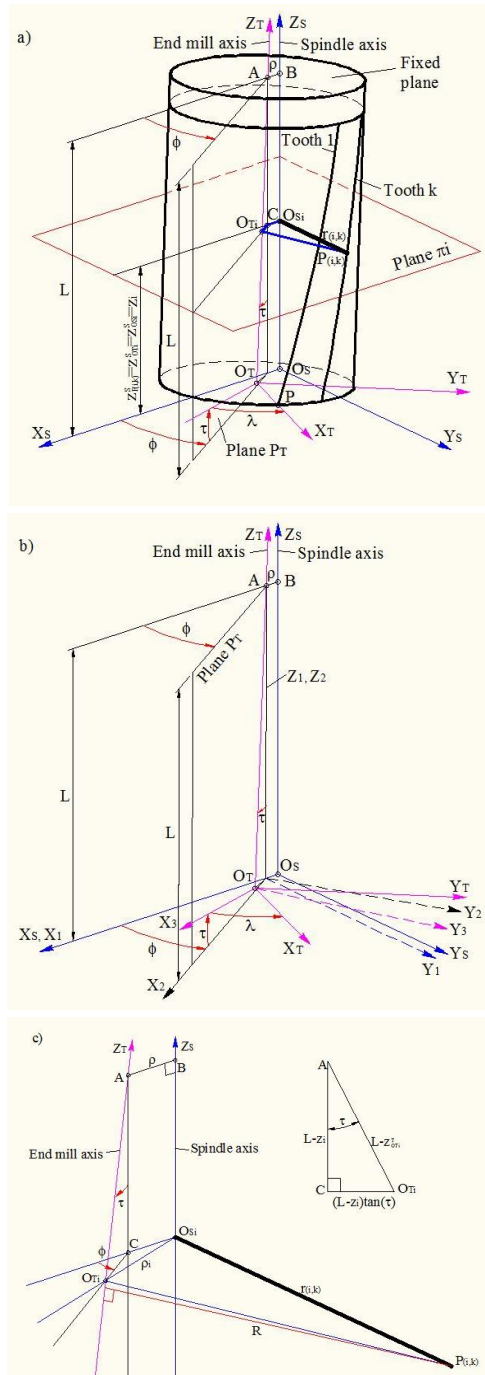


Figure 8. Tool setting error geometry (Arizmendi et al., 2009a)

Afterwards, solving equation (9) for z_{OTi}^T , the approximated $z_{P(i,k)}^T$ becomes:

$$z_{P(i,k)}^T \approx z_{O_i}^T = L - \frac{(L - z_i)}{\cos(\tau)} \quad (10)$$

From equation (5):

$$\beta_{(i,k)} \approx \frac{z_{O_i}^T \cdot \tan(\omega)}{R} = \left[L - \frac{(L - z_i)}{\cos(\tau)} \right] \frac{\tan(\omega)}{R} \quad (11)$$

When the angular position $\beta_{i,k}$ is determined, coordinates of every point of the cutting edge $P(i,k)$ in spindle system $X_S Y_S Z_S$ with equations (7) and (2) can be obtained. Through these coordinates, now can be carried out path defined by cutting edges point.

$$\begin{aligned} x_{P(i,k)}^T &= R \cdot \cos \left[\left(L - \frac{(L - z_i)}{\cos(\tau)} \right) \frac{\tan(\omega)}{R} + (k - 1) \frac{2\pi}{N_t} \right] \\ y_{P(i,k)}^T &= R \cdot \sin \left[\left(L - \frac{(L - z_i)}{\cos(\tau)} \right) \frac{\tan(\omega)}{R} + (k - 1) \frac{2\pi}{N_t} \right] \\ z_{P(i,k)}^T &= \frac{\left(L - \frac{(L - z_i)}{\cos(\tau)} \right) \frac{\tan(\omega)}{R}}{\tan(\omega)} = \left(L - \frac{(L - z_i)}{\cos(\tau)} \right) \end{aligned} \quad (12)$$

Definitive equations of point movement (13) that takes in consideration the error of tool setting through the parallel position change

$$\begin{aligned} \begin{bmatrix} x_{P(i,k)}^{(a)} \\ y_{P(i,k)}^{(a)} \\ z_{P(i,k)}^{(a)} \\ 1 \end{bmatrix} &= \begin{bmatrix} \cos(\alpha) & \sin(\alpha) & 0 & \frac{f}{2\pi} \alpha \\ -\sin(\alpha) & \cos(\alpha) & 0 & 0 \\ 0 & 0 & 1 & 0 \\ 0 & 0 & 0 & 1 \end{bmatrix} \begin{bmatrix} 1 & 0 & 0 & \rho \\ 0 & 1 & 0 & 0 \\ 0 & 0 & 1 & 0 \\ 0 & 0 & 0 & 1 \end{bmatrix} \begin{bmatrix} \cos(\phi) & -\sin(\phi) & 0 & 0 \\ \sin(\phi) & \cos(\phi) & 0 & 0 \\ 0 & 0 & 1 & 0 \\ 0 & 0 & 0 & 1 \end{bmatrix} \\ &= \begin{bmatrix} \cos(\tau) & 0 & -\sin(\tau) & L \cdot \sin(\tau) \\ 0 & 1 & 0 & 0 \\ \sin(\tau) & 0 & \cos(\tau) & L \cdot [1 - \cos(\tau)] \\ 0 & 0 & 0 & 1 \end{bmatrix} \begin{bmatrix} \cos(\lambda) & -\sin(\lambda) & 0 & 0 \\ \sin(\lambda) & \cos(\lambda) & 0 & 0 \\ 0 & 0 & 1 & 0 \\ 0 & 0 & 0 & 1 \end{bmatrix} \begin{bmatrix} R \cdot \cos \left[\left(L - \frac{(L - z_i)}{\cos(\tau)} \right) \frac{\tan(\omega)}{R} + (k - 1) \frac{2\pi}{N_t} \right] \\ R \cdot \sin \left[\left(L - \frac{(L - z_i)}{\cos(\tau)} \right) \frac{\tan(\omega)}{R} + (k - 1) \frac{2\pi}{N_t} \right] \\ L - \frac{(L - z_i)}{\cos(\tau)} \\ 1 \end{bmatrix} \quad (13) \end{aligned}$$

and axis tilt in the function of angle rotation α shown in matrix shape is obtained by replacing matrixes (12) in the expression (7).

Process for obtaining surface topography requires simulation of teeth paths for getting the roughness profile in every plane π_i . This simulation includes calculating position (x,y) every cutting edge point on discrete feed of rotation angle α . To generate a roughness profile on height z_i , intersection points between cutting edge paths have to be specified, and to know which tooth leaves its trail on a workpiece, a comparison must be carried through stages. Once when the roughness profile on every plane π_i along axial depth is established, all profiles are combined to form a surface topography. From figure 9-a all teeth marks can be noticed, and that from those 4 teeth only 2 perform cutting, or that to a certain height ($z_{borderI}$) only 1 tooth cuts (tooth 4), and from the next border ($z_{borderII}$), and further cutting is done by only 1 tooth, and that is tooth 4. In the area between these borders they are changing.

This crossing is called transition mark, and the appearance is called heterogeneity band (Figure 9-b).

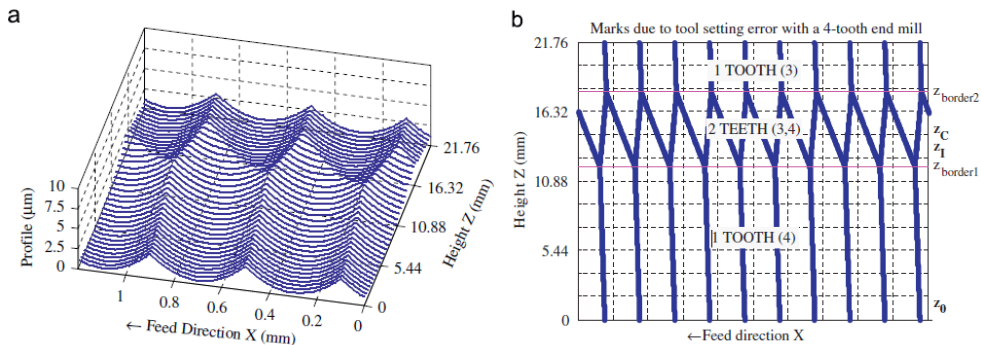


Figure 9. Surface topography of the milled surface (Arizmendi et al., 2009b)

5. Model that takes in consideration the measurement deviations of tooth mill

The main cause of measurement deviations is its production. As well as every other machine element, the tooth mirror measures are given at construction in certain tolerances and regardless on the fact that those tolerances can be very narrow, it can happen that in milling with small feed some of mill teeth do not pursue cutting. The same applies to oversharpened mills (Đorđević, 1991). Regardless if the mistake happened due to bad setting of the mill or due to development (or sharpening), if e.g. two teeth don't cut at all, the tooth that comes after them will process three times larger amounts of materials then it had to, so the resistances on that tooth will be much larger then expected, process of wearing more intensive, and the quality of the processed surface will be worse and more rough.

Measuring deviations of milling edge can be brought down on three basic (Đorđević, 1991): radial ($\Delta_{r,i}$), tangential ($\Delta_{t,i}$) and axial ($\Delta_{a,i}$), ($i \in 1, \dots, N_k$) (Figure 10), that format adequate angle deviation:

$$(\Delta\alpha_{k,k-1} = (k-1)2\pi / N_t - \alpha_{k-1,k})$$

On figure 10 a view from top of a mill with 4 teeth is shown. Hypothetically measuring deviations of a mill were selected so that the tooth 1 has no deviations. Tooth 2 contains

only radial deviations, while teeth 3 and 4 contain radial and tangential deviations. Specified deviations cause reduction or increase of angle α that in a ideal mill, with a mill that has 4 teeth is 90° . Axial deviations of tooth measures (deviations along mill axis) is not shown on the figure but can be assumed. If the teeth don't have same elevation, ie. height in comparison on some referent horizontal plane, or rather, some of mentioned teeth are not laying in the horizontal plane and unevenly are apart from it, among them is present axial measure deviations.

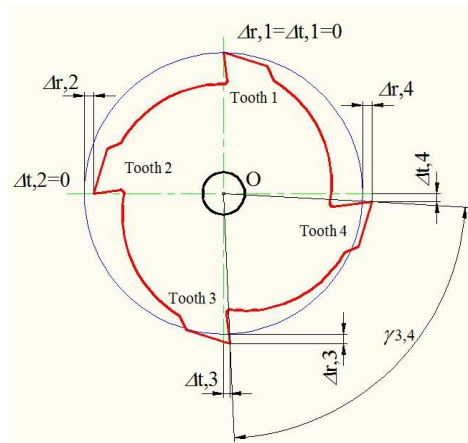


Figure 10. Example of measurement deviations of a 4 tooth mill (Đorđević, 1991)

Although it's clear that their influence exists, here the influence of tangential and axial deviations is neglected, because it's assumed that, in difference of radial, they don't have

considerable influence on topography of the milled surface at an extensive milling.

To bring in the influence of radial deviations in a pre-made model that takes in consideration the errors of setting the mill, primarily we will derive an expression for an effective cutting edge radius that takes the pre-specified error parameters of tool setting, and then introduce in the same the error due to mill measurement deviations.

The influence of tooth radial deviations on generating a milled surface is obtained by a simple addition of their values into the equation (13). By adding radial deviation $\pm \Delta r(i,k)$, point $P(i,k)$ moves to position $P'(i,k)$ (Figure 11). It is important to say that with the specified process some assumptions were made because of the clearly insignificant errors and easier calculations, so: $\pm \Delta r(i,k) = \pm \Delta' r(i,k)$. Also neglected was the change in mill diameter due to radial deviations by height z_i . So we get the matrix of coordinates of the point deviations on the

cutting edge of the mill tooth $P^{\alpha}_{\Delta(i,k)}$ that takes in consideration the deviations due to mill error settings and radial tooth deviations.

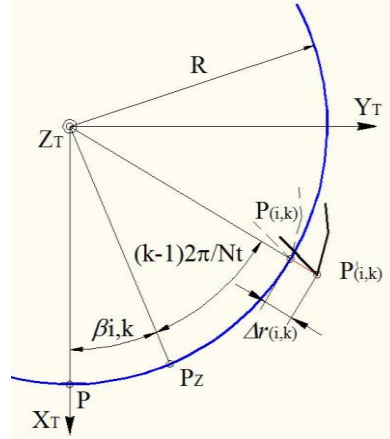


Figure 11. Radial deviation of the point $P_{(i,k)}$ on the cutting edge

$$\begin{bmatrix} x_{PA(i,k)}^{(\alpha)} \\ y_{PA(i,k)}^{(\alpha)} \\ z_{PA(i,k)}^{(\alpha)} \\ 1 \end{bmatrix} = \begin{bmatrix} \cos(\alpha) & \sin(\alpha) & 0 & \frac{f}{2\pi} \\ -\sin(\alpha) & \cos(\alpha) & 0 & 0 \\ 0 & 0 & 1 & 0 \\ 0 & 0 & 0 & 1 \end{bmatrix} \begin{bmatrix} 1 & 0 & 0 & \rho \\ 0 & 1 & 0 & 0 \\ 0 & 0 & 1 & 0 \\ 0 & 0 & 0 & 1 \end{bmatrix} \begin{bmatrix} \cos(\phi) & -\sin(\phi) & 0 & 0 \\ \sin(\phi) & \cos(\phi) & 0 & 0 \\ 0 & 0 & 1 & 0 \\ 0 & 0 & 0 & 1 \end{bmatrix} \begin{bmatrix} \cos(\tau) & 0 & -\sin(\tau) & L \cdot \sin(\tau) \\ 0 & 1 & 0 & 0 \\ \sin(\tau) & 0 & \cos(\tau) & L \cdot [1 - \cos(\tau)] \\ 0 & 0 & 0 & 1 \end{bmatrix} \\
 \begin{bmatrix} \cos(\lambda) & -\sin(\lambda) & 0 & 0 \\ \sin(\lambda) & \cos(\lambda) & 0 & 0 \\ 0 & 0 & 1 & 0 \\ 0 & 0 & 0 & 1 \end{bmatrix} \begin{bmatrix} (R \pm \Delta r_{(i,k)}) \cdot \cos \left[\left(L - \frac{(L - z_i)}{\cos(\tau)} \right) \frac{\tan(\omega)}{R} + (k-1) \frac{2\pi}{N_i} \right] \\ (R \pm \Delta r_{(i,k)}) \cdot \sin \left[\left(L - \frac{(L - z_i)}{\cos(\tau)} \right) \frac{\tan(\omega)}{R} + (k-1) \frac{2\pi}{N_i} \right] \\ L - \frac{(L - z_i)}{\cos(\tau)} \\ 1 \end{bmatrix} \quad (14)$$

6. Display of the error influence of the setting and production (wasting) of the tooth

To mathematically display the error influence of setting a mill and mill tooth wearing it is needed to inspect specific (characteristic) cases and introduce them in the listed model (equation 14).

The cutting and mill geometry regimes are taken from the work (Arizmendi et al., 2009a) and given in the table 1. Values of tooth radial deviations are entered so that in angle $\lambda=0^\circ$ and height of the cross-sectional plane of $z=0$ mm the least milled surface roughness is occurring. Thus obtained values are $\Delta_1=0,003$ mm, $\Delta_2=-0,005$ mm, $\Delta_3=-0,003$ mm and $\Delta_4=0,005$ mm.

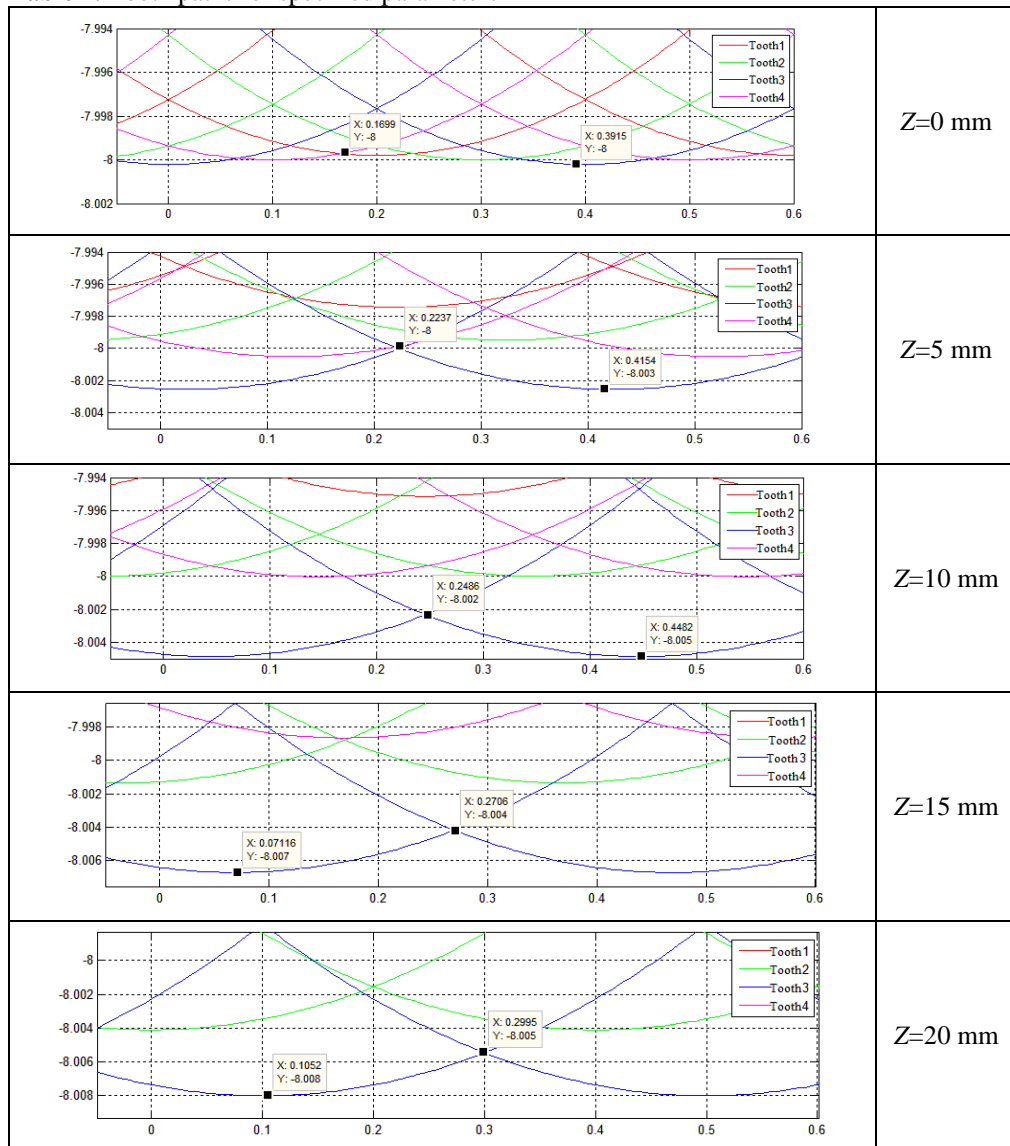
Table 1. Simulated cutting conditions

End mill radius	R = 8 mm	Cutter parallel axis offset	$\rho = 5 \mu\text{m}$
Cutter extending length	L= 32 mm	Tilt angle	$\tau = 0.005^\circ$
Number of teeth	Nt = 4 teeth	Locating angle	$\phi = 90^\circ$
Helix angle	$\omega = 30^\circ$	Locating angle	$\lambda = 0^\circ$
Axial depth	$a_p = 20 \text{ mm}$	Feed	$f = 0.4 \text{ mm}$

The following figures (Table 2) show the resulting trajectory of tooth mill depending

on the height of the observed cross-sectional plane in the range $z=0, 5, 10, 15, 20 \text{ mm}$.

Table 2. Tooth paths for specified parameters



The abscissa shows the feed, and ordinates show the mill radius, which the roughness maximum is measured from. Heights in the range from the mill top to the final axial height depth, or cover a total milling surface for height z .

In this way the analysis of possible axis positions of the mill (ρ , τ , ϕ) relative to the spindle axis, mill tooth position, and different values of deviation of the mill tooth diameter on the topography of the milled surface can be carried out.

From the listed figures the roughness change can be analysed, that is obviously smallest on the mill bottom and grows with size change. Likewise the diameter change, that changes from the bottom to the top and, at these parameters it gradually grows from 8 mm on the bottom to 8,008 mm on the top of the milled surface. Stacking these mill marks with different values of height, the topography of the whole milled surface for the mill with unequal tooth radiuses can be obtained. Likewise from the figures it can be noticed that on the top of the mill ($z=0$), all of the teeth participate in the milling process, while shortly (from the height $z=5$ mm), the

cutting is taken over tooth 3 and it, with height increase is the only performs cutting and forms the surface topography.

7. Conclusions

One of the factors that can degrade the esthetic surface quality is the so-called „tooling error“ that occurs when the tool axis is not matching the spindle axis. The second factor is the tooth radius difference that occurs due to bad mill making but also continuous and unequal spending of the mill tooth. This paper gives a review on the geometry of a milled surface and gives mathematical models for assessment of the topography of a milled surface that developed and improved over time. Starting from Martelloti's model, until the last. The work is simple, in the previous model with the error of clamping tools, introduced errors of wearing out a tooth. Based on the derived model, a short analysis of obtained results from where a error of clamping tools and tooth wearing is easily noticed on the quality (topography) of a milled surface.

References:

- Arizmendi, M., Fernandez, J., Gil, A., & Veiga, F. (2009a). Effect of tool setting error on the topography of surfaces machined by peripheral milling. *International Journal of Machine Tools & Manufacture*, 49, 36-52.
- Arizmendi, M., Campa, F. J., Fernandez, J., Lopez de Lacalle, L. N., Gil, A., Bilbao, E., . . . Lamikiz, A. (2009b). Model for surface topography prediction in peripheral milling considering tool vibration. *CIRP Annals - Manufacturing Technology*, 58, 93-96.
- Arizmendi, M., Fernandez, J., Gil, A., & Veiga, F. (2010a). Model for the prediction of heterogeneity bands in the topography of surfaces machined by peripheral milling considering tool runout. *International Journal of Machine Tools & Manufacture*, 50, 51-64.
- Arizmendi, M., Fernandez, J., Gil, A., & Veiga, F. (2010b). Identification of tool parallel axis offset through the analysis of the topography of surfaces machined by peripheral milling. *International Journal of Machine Tools and Manufacture*, 50, 1097-1114.
- Babin, T. S., Lee, J. M., Sutherland, J. W., & Kapoor, S. G. (1985). A model for end milled surface topography. Paper presented at the Proceedings of the 13th North American Manufacturing Research Conference, SME (pp. 362-368).

- Babin, T. S., Sutherland, J. W., & Kapoor, S. G. (1986). On the geometry of end milled surfaces. Paper presented at the Proceedings of the 14th North American Manufacturing Research Conference, SME (pp. 168-176).
- Dorđević, Z. (1991). *Novi pristup razvoju sistema upravljanja alatnim mašinama* (Unpublished magistar thesis). Svetozar Marković University, Faculty of Mechanical Engineering, Kragujevac.
- Dotcheva, M., Dotchev, K., & Popov, I. (2013). Modelling and Optimisation of Up-and Down-Milling Processes for a Representative Pocket Feature. *International Journal of Precision Engineering and Manufacturing*, 14(5), 703-708.
- Ehmann, K. F., & Hong, M. S. (1994). A generalized model of the surface generation process in metal cutting. *CIRP Annals - Manufacturing Technology*, 43(1), 483-486.
- Gao, T., Zhang, W. H., Qiu, K. P., & Wan, M. (2006). Numerical simulation of machined surface topography and roughness in milling process. *ASME Journal of Manufacturing Science and Engineering*, 128(1), 96-103.
- Ismail, F., Elbestawi, M. A., Du, R., & Urbasik, K. (1993). Generation of milled surfaces including tool dynamics and wear. *ASME Journal of Engineering for Industry*, 115, 245-252.
- Kline, W. A., & DeVor, R. E. (1983). The effect of runout on cutting geometry and forces in end milling. *International Journal of Machine Tool Design and Research*, 23, 123-140.
- Kline, W. A., DeVor, R. E., & Shareef, I. A. (1982). The prediction of surface accuracy in end milling. *ASME Journal of Engineering for Industry*, 104, 272-278.
- Li, H. Z., & Li, X. P. (2005). A numerical study of the effects of cutter runout on milling process geometry based on true tooth trajectory. *International Journal of Advanced Manufacturing Technology*, 25, 435-443.
- Martellotti, M. E. (1941). An analysis of the milling process. *Transactions of the American Society of Mechanical Engineers*, 63, 677-700.
- Omar, O. E. K. K., El-Wardany, T., Ng, E., & Elbestawi, M. A. (2007). An improved cutting force and surface topography prediction model in end milling. *International Journal of Machine Tools and Manufacture*, 46, 1263-1275.
- Ranganath, S., & Sutherland, J. W. (2002). An improved method for cutter runout modeling in the peripheral milling process. *Machining Science and Technology*, 6(1), 1-20.
- Ryu, S. H., Lee, H. S., & Chu, C. N. (2003). The form error prediction in side wall machining considering tool deflection. *International Journal of Machine Tools and Manufacture*, 43, 1405-1411.
- Schmitz, T. L., Couey, J., Marsh, E., Mauntler, N., & Hughes, D. (2007). Runout effects in milling: surface finish, surface location error, and stability. *International Journal of Machine Tools and Manufacture*, 47, 841-851.
- Stori, J. A., Wright, P. K., & King, C. (1999). Integration of process simulation in machining parameter optimization. *Journal of Manufacturing Science and Engineering*, 121, 134-143.

Jasmina Dedić

Secondary school "Grigorije
Božović" Zubin Potok
Serbia
jasminavdedic@hotmail.com

Dragan Lazarević

University of Priština,
Faculty of Technical
Sciences
Serbia
dragan.lazarevic@pr.ac.rs

Bogdan Nedić

University of Kragujevac,
Faculty of Engineering
Serbia
nedic@kg.ac.rs

Milan Mišić

Higher Technical School of
Professional Studies Zvečan,
Serbia
m.misic@vts-zvecan.edu.rs

Živče Šarkoćević

University of Priština,
Faculty of Technical
Sciences
Serbia
zivce.sarkocevic@pr.ac.rs
